Electronic Supporting Information:

^{27}Al MAS NMR of Cu-containing SSZ-13 zeolites

Figure S1 displays the ^{27}Al MAS NMR spectra acquired for the two Cu-loaded SSZ-13 zeolites. Both spectra are dominated by a signal at 58 ppm, corresponding to tetrahedrally-coordinated Al species. A very weak signal is found however, for the Cu-SSZ-13(67) zeolite, at c.a. 0 ppm, of octahedral Al, indicating the presence of very small amounts of extra-framework Al species (see Table 1).

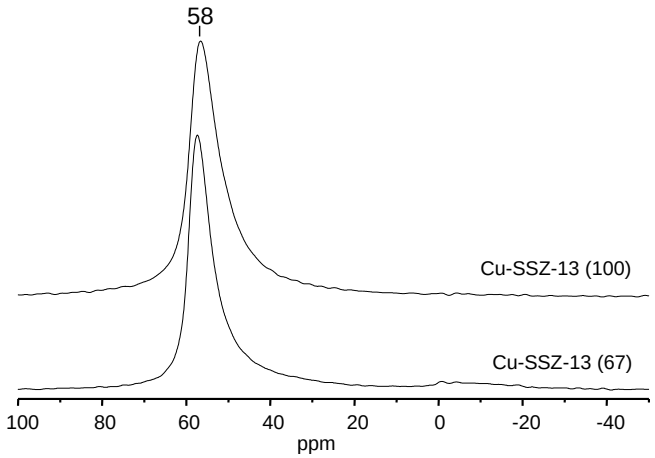

Figure S1. ^{27}Al MAS NMR spectra of Cu-SSZ-13 (67) and Cu-SSZ-13 (100) zeolites.

X-ray diffraction (XRD) of Cu-containing SSZ-13 zeolites

The XRD patterns (Figure S2) indicate that the crystallinity of the zeolite is maintained.

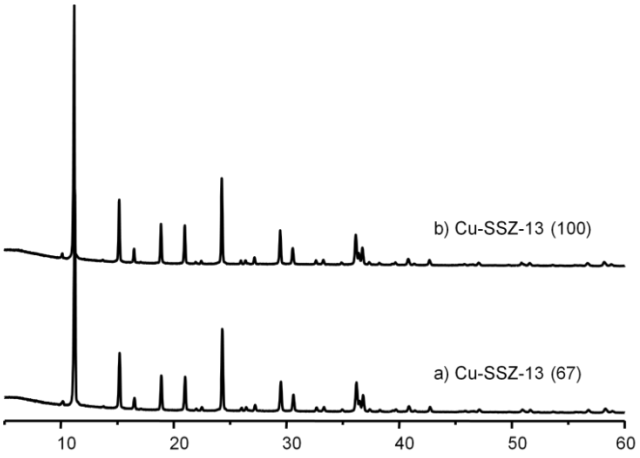

Figure S2. XRD patterns of Cu-SSZ-13 (67) (a) and Cu-SSZ-13 (100) (b) zeolites.

Detailed information on the theoretical calculations

Cu-exchanged model

The static geometry optimization results in a four-folded coordination for the Cu-SSZ-13 system (see Figure S3) with Cu-O separations ranging from 2.04 to 2.30 Å and a significantly distorted local environment, i.e. the six-membered ring.

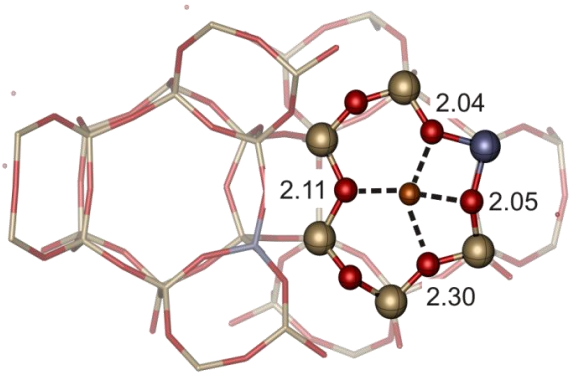

Figure S3. Optimized Cu-SSZ-13 structure with special indication of the local geometry of the metal ion. Relevant Cu-O distances are given in Å.

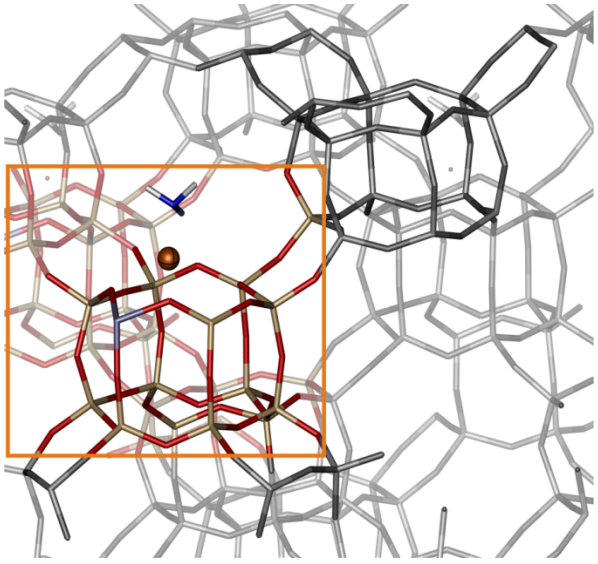

Figure S4. Periodic structure of a Cu-exchanged SSZ-13 zeolite used for the first-principles simulations.

H-exchanged models

For the proton-exchanged SSZ-13 zeolites (H-SSZ-13), periodic models were constructed containing two acidic protons (due to the double Si to Al substitution) and hence 110 atoms (the periodic structure is depicted in Figure S5). Two framework positions were distinguished, in particular the O(1) and O(2) positions corresponding with the low- and high-frequency band, respectively.

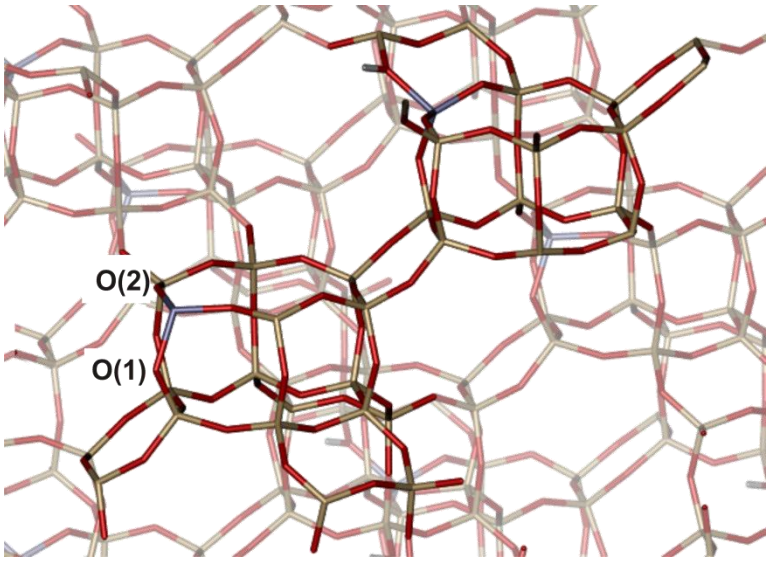

Figure S5. Periodic structure of a H-exchanged (proton not shown) SSZ-13 zeolite used for the first-principles simulations. Two different framework positions, O(1) and O(2), are indicated.

IR Simulations

After the geometry optimization, IR properties are calculated using two different methods: a static normal mode analysis (NMA) using the optimized geometry and a Fourier-based technique with input from molecular dynamics (MD) simulations. The NMA and MD simulations were performed applying the same computational details used for the geometry optimizations, however all atoms were described at the GPW level.

Static NMA. A partial Hessian analysis was performed for the NMA calculations where only the relevant portion of the chemically active center - i.e. the Cu^{2+} ion, the ammonia molecule and a single six-membered ring in which the Lewis or Brønsted acid site is located - is taken into account, and all other atoms were fixed. For the $[Cu(NH_3)_4]^{2+}$ complex, the atoms of the six-membered ring were not included in the NMA analysis since they interact little with the complex. The focus of this study is on the region above 1200 cm^{-1} and hence there is no need to include global motions which are found at much lower wavenumbers.

Molecular Dynamics. The MD calculations were performed on all atoms. After 2 ps equilibration with the canonical sampling through velocity rescaling thermostat,[1] the more robust Nosé–Hoover thermostat[2] was used for 13 ps with a timestep of 0.5 fs for the Cu-containing zeolites while the protonated SSZ-13 were all simulated for 32 ps with the same time step. The temperature of the simulations was held to 600 K in accordance with experiment. All post-processing of the MD simulations was done using the program MD-tracks.[3]

To calculate the peak positions for the IR spectrum from the MD simulation, the velocity power spectrum (VPS) is determined by the Fourier transforms of the velocities, which are squared and summed.[4]

$$I_{VPS}(\omega) = \lim_{t\to\infty} \frac{1}{t} \sum_{i=1}^{N} \sum_{\alpha=x,y,z} \left| \int_0^t v_{i,\alpha}(t) \mathrm{e}^{-\mathrm{i}\omega t}\, dt \right|^2$$

This is related to the IR spectrum since this is the Fourier transform of the time derivative of the dipole moment $\mu_\alpha = \sum_i q_i R_{i\alpha}$.

$$I_{IR}(\omega) = \lim_{t\to\infty} \frac{1}{t} \sum_{\alpha=x,y,z} \left| \int_0^t \frac{d\mu_\alpha(t)}{dt} \mathrm{e}^{-\mathrm{i}\omega t}\, dt \right|^2$$

The derivative of the dipole moment is indeed very much related to the velocity. Hence, the VPS is related to the IR spectrum and contains even more information.

The theoretical spectra of the NH_3@Cu^{2+} site, NH_3@Brønsted site (O1), NH_3@ Brønsted site (O2) and $(NH_3)_4$@Cu^{2+} site spectra in the region 200-1200 cm^{-1} are compared in Figure S6.

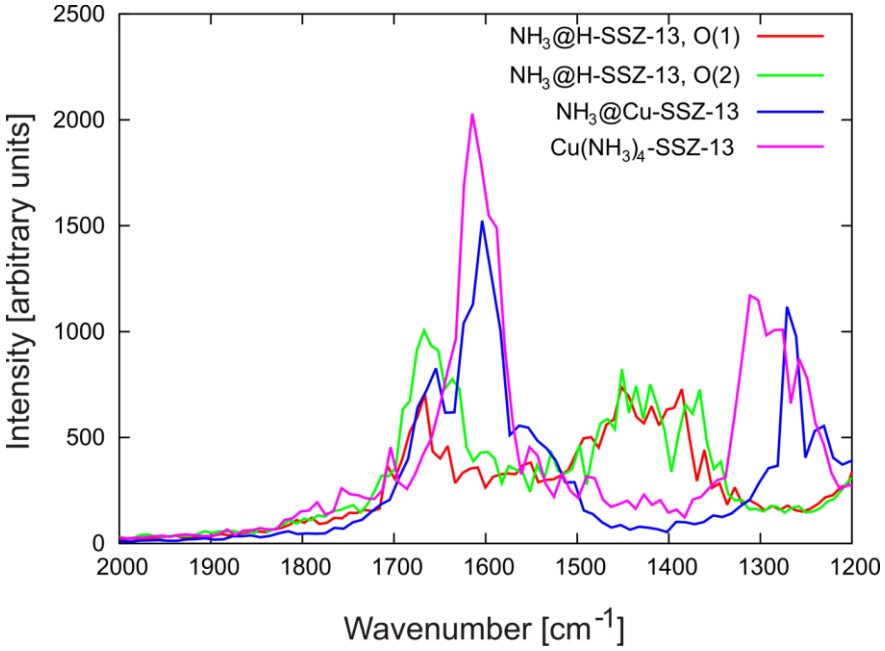

Figure S6. Theoretical spectra derived from MD simulations at 600 K of NH_3@Brønsted site (O1) (red), NH_3@Brønsted site (O2) (green), NH_3@Cu^{2+} site (blue) and $(NH_3)_4$@Cu^{2+} site (pink) in the region 2000-1200 cm^{-1}.

Table S1. Theoretical frequencies (in cm^{-1}) of the ammonia-adsorbed structures, depicted in Figure 3. Comparison between the NMA and MD-based results.

	$\nu_{theor,NMA}$ (cm^{-1})		$\nu_{theor,MD}$ (cm^{-1})		**Assignment**
	O(1)	**O(2)**	**O(1)**	**O(2)**	
NH_3@Brønsted site	-	1480	1432	1455	$\delta(NH_4^+)_{as}$
	-	1387	1370	1368	$\delta(NH_4^+)_s$
	$[Cu(NH_3)]^{2+}$	**$[Cu(NH_3)_4]^{2+}$**	**$[Cu(NH_3)]^{2+}$**	**$[Cu(NH_3)_4]^{2+}$**	
NH_3@Cu^{2+} site	1632	1621	1601	1606	$\delta(NH_3)_{as}$
	1537		1535		hydrogen-bonded $\delta(NH_3)_{as}$ in $[Cu\text{-}NH_3]^{2+}$
	1261	1291	1271	1285	NH_3 wagging

UV-Vis-NIR DRS Spectroscopy of Cu-containing SSZ-13 zeolites

The UV-Vis spectrum acquired for the Cu-SSZ-13(67) zeolite, depicted in Figure S7, shows the presence of isolated Cu^{2+} ions (ca. 12000 d–d and 47500 cm^{-1} charge transfer (CT) O → Cu),[5] whereas for the Cu-SSZ-13(100) zeolite a new band appears at 40000 cm^{-1}, attributed to the formation of isolated CuO particles.[6]

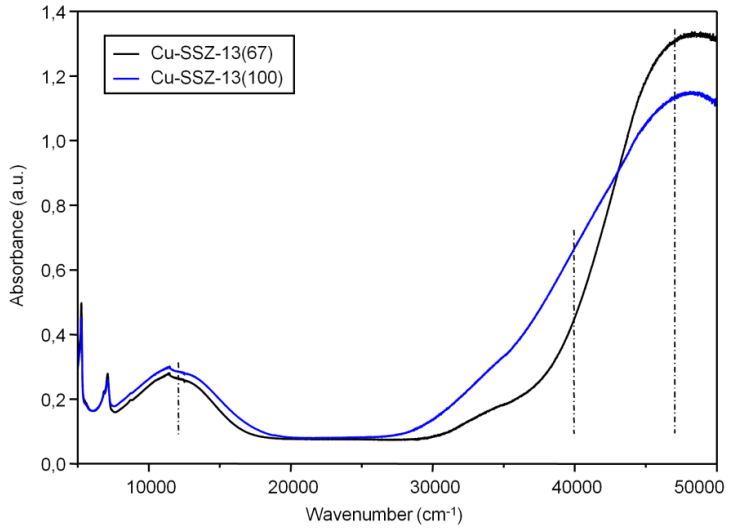

Figure S7. UV-Vis spectra of Cu-SSZ-13 (67) (black line) and Cu-SSZ-13 (100) (blue line) zeolites.

Cu-K edge EXAFS of Cu-containing SSZ-13 zeolites

Comparison of the EXAFS data (see Figure S8 and Table S2) shows a decrease in the intensity of the feature at ~1.96 Å for the Cu-SSZ-13(100) zeolite, indicating a slight reduction in the number of isolated Cu^{2+} ions,[7] together with the appearance of a new feature at ~3 Å. This new feature is due to a Cu-Cu contribution, and indicates the presence of small amounts of CuO in the Cu-SSZ-13(100) sample,[8] in accordance with the previous UV-Vis results.

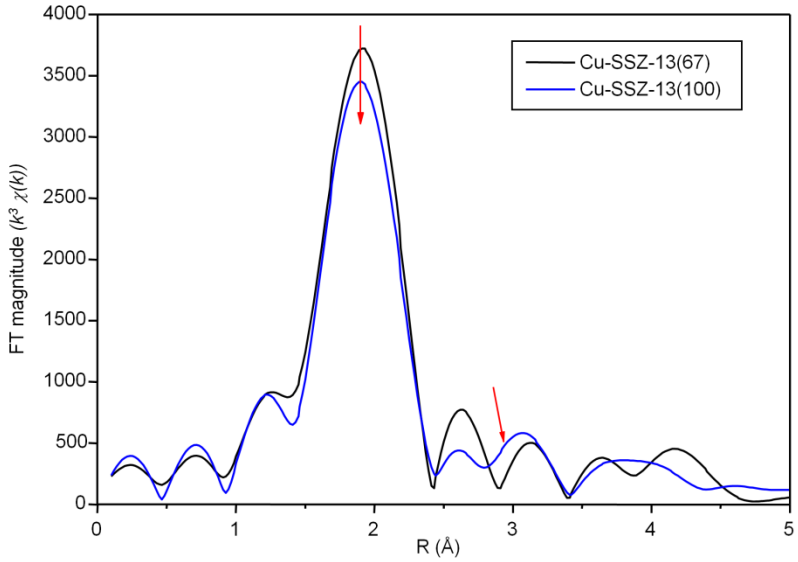

Figure S8. Fourier transform of $k^3\chi(k)$ EXAFS data for Cu-SSZ-13 (67) (black line) and Cu-SSZ-13 (100) (blue line) (solid line) zeolites.

Table S2. EXAFS parameters for Cu–O derived from a first shell fit of the data in k-space. Estimated errors (fitting) are listed in brackets below (±)

	R (Å)	***N***	**$2\sigma^2$ (Å^2)**	**E_f (eV)**	**R-factor**
Cu-SSZ-13 (67)	1.96	3.1	0.009	-1.15	
	(0.02)	(0.305)	(0.006)	(1.007)	24.18
Cu-SSZ-13 (100)	1.95	3.0	0.007	-0.45	
	(0.02)	(0.385)	(0.009)	(1.455)	23.37

R-factor values are calculated using the following formula:

$$R_{exafs} = \sum_{i}^{N} 1\ \sigma_i\left(\left|\chi_i^{exp}(k) - \chi_i^{th}(k)\right|\right) \text{ x } 100\%$$

N_2 sorption measurements of Cu-containing SSZ-13 zeolites

As shown in Table S3, N_2 sorption measurements basically show the same results; both Cu-loaded zeolites present a typical type I isotherm, corresponding to a fully microporous material, so that the presence of an additional mesopore system in Cu-SSZ-13(100), produced as a consequence of framework dealumination, can also be ruled out.

Table S3. BET surface area and micropore volume, determined by N_2 adsorption, and crystal size, obtained from Scanning Electron Microscopy (SEM) images, of Cu-SSZ-13 (67) and Cu-SSZ-13 (100) zeolites.

	A_{BET} (m^2/g)	$V_{\mu p}$ (cm^3/g)	Crystal size (μm)
Cu-SSZ-13 (67)	775	0.27	8-10
Cu-SSZ-13 (100)	765	0.26	8-10

Scanning Electron Microscopy (SEM) of Cu-containing SSZ-13 zeolites

Identical results were also obtained by SEM (see Table S3), ruling out the presence of smaller crystallites in Cu-SSZ-13(100) or a change in morphology, which could be also a possible reason of the enhanced reactivity.

References

1. G. Bussi, D. Donadio and M. Parrinello, *J. Chem. Phys.*, 2007, **126**, 14101.

2. S. Nosé, *Mol. Phys.*, 1984, **52**, 255; S. Nosé, *J. Chem. Phys.*, 1984, **81**, 511.

3. T. Verstraelen, M. Van Houteghem, V. Van Speybroeck and M. Waroquier, *J. Chem. Inf. Model.*, 2008, **48**, 2414.

4. M. Van Houteghem, T. Verstraelen, D. Van Neck, C. Kirschhock, J. A. Martens, M. Waroquier and V. Van Speybroeck. *J. Chem. Theo. Comput.*, 2011, **7**, 1045, and references herein.

5. M. H. Groothaert, J. A. Bokhoven, A. A. Battiston, B. M. Weckhuysen and R. A. Schoonheydt, *J. Am. Chem. Soc.*, 2003, **125**, 7629.

6. A. El-Trass, H. ElShamy, I. El-Mehasseb and M. El-Kemary, *Appl. Surf. Sci.*, 2012, **258**, 2997.

7. S. Bordiga, E. Groppo, G. Agostini, J. A. van Bokhoven and C. Lamberti, *Chem. Rev.*, 2013, **113**, 1736.

8. W. Grunert, N.W. Hayes, R.W. Joyner, E.S. Shpiro, M.R.H. Siddiqui and G.N. Baeva, *J. Phys. Chem.*, 1994, **98**, 10832.